Global observations of the carbon budget 2. CO_2 column from differential absorption of reflected sunlight in the 1.61 μm band of CO_2

D. M. O'Brien and P. J. Rayner
CSIRO Atmospheric Research, Aspendale, Australia

Received 9 March 2001; revised 18 December 2001; accepted 21 December 2001; published 25 September 2002.

[1] This paper investigates the impact of uncertainty in atmospheric composition and state upon the feasibility of measuring the CO_2 column from spectral analysis of sunlight reflected to space in the 1.61 μm absorption band of CO_2. In principle, measurements of clear sky radiance at two frequencies, one where CO_2 absorbs strongly and the other weakly, allow the difference between the optical thicknesses of the atmosphere at the two frequencies to be determined precisely. That difference, denoted by L, is a linear functional of the CO_2 density profile, which depends strongly on the CO_2 amount and only weakly upon its vertical distribution, thus suggesting that the CO_2 column may be estimated from L. A simple model for the radiance reflected to space is used to estimate the magnitude of the error in the CO_2 column inferred from L when the atmosphere contains thin cloud and aerosol. It emerges that measurements in two channels in the 1.61 μm CO_2 absorption band are too sensitive to cloud and aerosol to allow the CO_2 column to be inferred with precision better than a few percent in the presence of thin cloud and aerosol. However, simultaneous measurements of optical thickness in the nearby 1.27 μm absorption band of O_2 are tightly correlated with those for CO_2, even in the presence of aerosol and thin cirrus, and therefore may allow the CO_2 column to be determined relative to the O_2 column, provided that the latter is known independently from surface pressure. The correlation between O_2 and CO_2 optical thicknesses depends upon the mean scattering height, but this quantity may be estimated with sufficient accuracy from radiances measured in the O_2 band. A prototype algorithm is developed to estimate the CO_2 column from data in two CO_2 channels and three O_2 channels. The algorithm is used to estimate the probable bias and standard error of measurements of CO_2 column from space under conditions where the optical thicknesses of aerosol and cirrus may be as large as 0.2 and 0.1, respectively, and where the temperature profile is known to within ±1 K. The simulations suggest that the error in the estimated CO_2 column caused by these sources is approximately 0.5%. This conclusion is interpreted cautiously because the analysis assumes inter alia that the spectroscopic properties of both CO_2 and O_2 are known accurately, that the surface reflectance and the scattering properties of aerosol and cirrus vary predictably between 1.27 μm and 1.61 μm, and that difficult technical issues associated with high spectral resolution measurements can be resolved. Nevertheless, the importance of global measurements of CO_2 is such that the method warrants further investigation. *INDEX TERMS:* 0322 Atmospheric Composition and Structure: Constituent sources and sinks; 0394 Atmospheric Composition and Structure: Instruments and techniques; 0360 Atmospheric Composition and Structure: Transmission and scattering of radiation; *KEYWORDS:* global, CO_2, differential absorption, sunlight, feasibility

Citation: O'Brien, D. M., and P. J. Rayner, Global observations of the carbon budget, 2, CO_2 column from differential absorption of reflected sunlight in the 1.61 μm band of CO_2, *J. Geophys. Res.*, *107*(D18), 4354, doi:10.1029/2001JD000617, 2002.

1. Introduction

[2] Despite the importance of monitoring the sources and sinks of CO_2 and other greenhouse gases in the atmosphere, the prevailing wisdom for many years has been that the precision of measurements from space would be too poor to help reduce the uncertainty in the carbon budget. Indeed, measurements of CO_2 volume mixing ratio at baseline air pollution stations, such as Cape grim, typically have errors around 0.1 ppmv, whereas measurements from space are unlikely to have precision better than 1–2 ppmv. Never-

0148-0227/02/2001JD000617$09.00

theless, satellites offer good spatial coverage and high temporal resolution, so the random component of the error in individual measurements should cancel in regional and temporal averages. The impact of such measurements of the CO_2 column was investigated by *Rayner and O'Brien* [2001], who demonstrated that monthly means over $8^\circ \times 10^\circ$ regions would reduce substantially the uncertainty in the global distribution of sources and sinks of CO_2, provided that the accuracy of the monthly mean volume mixing ratios is approximately 1–2 ppmv. Similar work in progress by Denning et al. (personal communication, 2000) supports this conclusion. The question then arises as to whether such measurements are possible.

[3] Of the candidate technologies, the more promising are analysis of thermal infrared radiation emitted to space in an emission band of CO_2 (for example, the 4.3 μm band), differential absorption of sunlight reflected from the earth in an absorption band of CO_2, and differential absorption with a tunable laser as the source rather than sunlight. Each of these options requires careful analysis, and it is likely that comprehensive mapping of CO_2 will require the current surface network of gas sampling stations together with all three of the technologies mentioned. *Engelen et al.* [2001] have begun the analysis of the thermal infrared option, while McMillin et al. (personal communication) have conducted sensitivity analyses for both the Atmospheric Infra-Red Sounder (AIRS) and the High Resolution Infrared Sounder HIRS. *Tolton and Plouffe* [2001] considered a simple radiometer in the CO_2 absorption band at 1.61 μm, while *Buchwitz et al.* [2000] assess the potential of the SCIAMACHY instrument to measure the CO_2 column. This paper examines differential absorption of reflected sunlight in the 1.61 μm band of CO_2.

[4] While the emphasis of the paper is on the errors caused by thin cloud and aerosol, the discussion requires a basic concept for the instrumentation. We assume a spectrometer, such as a Fabry-Peron etalon, capable of making radiance measurements with high spectral resolution (≈ 0.02 cm^{-1}) and high signal-to-noise ratio in a few selected channels in the CO_2 band at 1.61 μm. Because diffuse reflectance from the oceans is very low at 1.61 μm (typically $\approx 0.3\%$), we assume that the spectrometer scans towards sun-glint over the oceans. Furthermore, because sunlight reflected from glint is Doppler shifted, we assume that the spectrometer may be tuned dynamically to compensate for Doppler shifts. Finally, we will assume that the spectrometer has additional channels in the O_2 band at 1.27 μm in order to provide data to compensate for the effects of scattering by cloud and aerosol. The rationale for these requirements will be outlined in later sections.

[5] Because measurement of CO_2 from space is a complex issue, beyond the scope of a single paper, this study is exploratory. We use a simple model for the radiance reflected to space to investigate the sensitivity of the radiance to factors including the surface reflectance, the temperature profile, and the amount and vertical distribution of thin cloud and aerosol. Thus this paper investigates the limitations imposed by uncertain atmospheric conditions, leaving to later publications the technical feasibility of the measurements and the impact of instrumental noise. Furthermore, because the uncertainty associated with atmospheric scattering appears to be the most critical factor, we assume for this study that CO_2 is uniformly mixed in the atmosphere, thereby allowing us to focus on scattering and relegate the complications caused by nonuniform volume mixing ratio. Clearly this assumption must be eliminated in later studies.

[6] We show that measurements in two channels in a near infrared CO_2 band, one strongly absorbing and the other weakly so, are too sensitive to scatterers to allow the CO_2 column to be determined with accuracy better than $\approx 2-3\%$, even in very clear atmospheric conditions where the total optical thickness of cloud and aerosol does not exceed 0.04. However, when three extra channels in a nearby absorption band of O_2 at 1.27 μm are included, substantially better accuracy is possible, provided that the reflectance of the surface and the optical properties of the scattering material vary in a predictable way between the CO_2 and O_2 bands. We propose an algorithm to recover the CO_2 column from radiances in the CO_2 and O_2 channels, and we test the algorithm with simulated data. Radiances are computed for a variety of surface and scattering conditions and are passed through the inversion algorithm to produce statistics (bias and variance) of the error. In a companion paper, we investigate the impact that the data are likely to have upon mapping sources and sinks of CO_2.

2. Basic Theory

[7] The principle underlying differential absorption is very simple. Rays from the sun with frequencies in absorption bands of CO_2 are attenuated as they penetrate the atmosphere, reflect from the surface and travel back to space. The reflected radiance depends on the brightness of the reflecting surface, but the ratio of two radiances, measured at frequencies with differing attenuation by CO_2, is simply related to the amount of CO_2 along the path traversed by the rays and is independent of the surface albedo. Thus one might expect that measurements at two frequencies would suffice to determine the CO_2 content of the atmosphere.

[8] To see this more formally, suppose that the radiance reflected to space is measured at frequencies ν_0, ν_1,... with increasing absorption by CO_2. In the absence of scattering by the atmosphere, the radiance I_j reflected to space at frequency ν_j is

$$I_j = (4\pi)^{-1} Fr \sec\theta_r \exp(-m\tau_j),$$

where F is the solar flux density at the top of the atmosphere, τ_j is the optical thickness of the atmosphere at frequency ν_j, m is the air mass factor that accounts for slant paths followed by the photons,

$$m = |\sec\theta_i| + |\sec\theta_r|,$$

and θ_i and θ_r are the angles of incidence and reflection at the surface. The factor r denotes the bidirectional reflectance distribution function (BRDF) of the surface, which we call more simply the reflectance. The normalization of r used here is nonstandard but well suited for modeling surfaces that do not reflect isotropically. For an

isotropic reflector (a Lambertian surface), one normally would write

$$I_j = \pi^{-1} F \cos\theta_i A \exp(-m\tau_j),$$

where A is the Lambertian albedo, in which case

$$r = 4A\cos\theta_i \cos\theta_r.$$

If the frequencies ν_0, ν_1,... are sufficiently close, then the reflectance and the solar flux density will be the same for all, so the ratio

$$X_j = I_j/I_0 = \exp[-m(\tau_j - \tau_0)] \quad (1)$$

depends only on the geometrical configuration (through m) and upon the difference between the optical thicknesses at frequencies ν_j and ν_0. For most satellite platforms, the geometry is known with high accuracy, so a measurement of the radiances I_j and I_0 provides a direct measurement of the optical path difference,

$$L_j = \tau_j - \tau_0.$$

Furthermore, if the frequencies are chosen in the near infrared, so that Rayleigh scattering and thermal emission may be neglected, and if absorption by other gases (such as water vapor) is either negligible or constant over the range from ν_0 to ν_j, then the optical path difference L_j is directly related to the CO_2 density profile $N(z)$ (in mol m^{-3}). Indeed,

$$L_j = \int_0^\infty dz N(z)[k(\nu_j, p, T) - k(\nu_0, p, T)], \quad (2)$$

where $k(\nu_j, p, T)$ (in m^2 mol^{-1}) is the specific absorption of CO_2, known from laboratory measurements, and p and T denote the pressure and temperature profiles. Equation (2) shows that a measurement of L_j is a linear functional of the CO_2 density profile with kernel determined by the specific absorption of CO_2, which in turn depends on pressure and temperature.

[9] Although we will restrict the analysis of this paper to the case in which CO_2 is mixed uniformly throughout the atmosphere, it is worth noting how L_j depends on the CO_2 column in a general setting. If we let

$$u = \int_0^\infty dz N(z)$$

denote the CO_2 column amount (in mol m^{-2}), $n(z)$ denote a reference density profile for CO_2 normalized so that

$$\int_0^\infty dz n(z) = 1,$$

and $\varepsilon(z)$ denote departures from the reference profile, then

$$N(z) = un(z)(1 + \varepsilon(z)) \quad \text{and} \quad \int_0^\infty dz n(z)\varepsilon(z) = 0.$$

It follows easily that

$$L_j = A_j u(1 + B_j), \quad (3)$$

where A_j is the specific absorption difference weighted by the reference profile,

$$A_j = \int_0^\infty dz n(z)[k(\nu_j, p, T) - k(\nu_0, p, T)],$$

and B_j is a similarly weighted mean of $\varepsilon(z)$,

$$B_j = A_j^{-1} \int_0^\infty dz n(z)\varepsilon(z)[k(\nu_j, p, T) - k(\nu_0, p, T)].$$

Generally, B_j will be small compared with unity. Indeed, if it were not for the variation of the specific absorption with pressure and temperature, B_j would be identically zero for any density profile of CO_2. Thus equation (3) shows that L_j depends primarily on the CO_2 column and only weakly on the departures of the CO_2 density profile from the reference profile.

3. Issues

[10] In reality, measurement of the CO_2 optical path difference and its analysis to determine CO_2 density profile is far more complex. Not only are there acute technical problems concerning the feasibility of the measurements, but also the simple concept outlined above neglects important processes, such as scattering by cloud and aerosol, and assumes that ancillary data, such as the optical properties of CO_2 and the temperature profile of the atmosphere, are known reliably. Furthermore, analysis of measurements of optical path difference to derive useful information about the global distribution of sources and sinks will require models of the sources, sinks and transport mechanisms between them, and such models will introduce additional uncertainties. In this section we canvass these issues briefly, while in the remainder of the paper we will focus on the uncertainties arising from atmospheric effects.

3.1. Scattering by Cloud and Aerosol

[11] Photons scattered by aerosol and cloud generally traverse shorter paths through the atmosphere than photons reflected from the surface, and therefore suffer less absorption by CO_2. Consequently, analysis of the ensemble of all rays (reflected and scattered) as though they had been reflected from the surface will lead to an underestimate of the amount of CO_2. The higher the scatterer in the atmosphere, the greater will be the underestimate. If the amount of cloud and aerosol were known, the analysis could be adjusted to compensate for this effect, but in reality clouds and aerosol are highly variable and their scattering properties uncertain, so some error is inevitable. Data from thick clouds can be trapped and discarded reliably, but thin, subvisual cloud (such as cirrus) poses a serious problem.

[12] A first analysis of the issue may be made with a very simple model of the atmosphere, because at 1.61 μm Rayleigh scattering may be neglected and only conditions

with optically thin aerosol and cloud need be considered, in which case the scattered radiance is dominated by the component singly scattered. Thus the radiance I reflected to space consists of three components, I_s reflected from the surface, I_a scattered by aerosol and I_c scattered by cloud,

$$I = I_s + I_a + I_c,$$

where temporarily the frequency index has been omitted for clarity. Furthermore, if the aerosol is assumed to lie below the cloud and both are assumed to be concentrated in layers that are thin in comparison with the scale height of CO_2, then the contributions to the radiance are

$$I_s = \frac{F}{4\pi}\sec\theta_r r e^{-m\tau_g} e^{-m\tau_a} e^{-m\tau_c}, \tag{4}$$

$$I_a = \frac{F}{4\pi}\sec\theta_r p_a \varpi_a e^{-m\tau_{ga}}\left(\frac{1-e^{-m\tau_a}}{m}\right) e^{-m\tau_c}, \tag{5}$$

$$I_c = \frac{F}{4\pi}\sec\theta_r p_c \varpi_c e^{-m\tau_{gc}}\left(\frac{1-e^{-m\tau_c}}{m}\right), \tag{6}$$

where τ_g, τ_a and τ_c denote the optical thicknesses of absorbing gas (CO_2), aerosol and cloud measured along a vertical path from the surface to space, τ_{ga} and τ_{gc} denote the optical thicknesses of gas above the aerosol and cloud layers, and p_a and p_c denote the scattering phase functions of aerosol and cloud, with ϖ_a and ϖ_c the corresponding single scattering albedos. Because the optical thicknesses of aerosol and cloud are assumed to be small, the expressions for I_a and I_c may be approximated by

$$\begin{aligned} I_a &= \frac{F}{4\pi}\sec\theta_r (p_a \varpi_a \tau_a) e^{-m\tau_{ga}} e^{-m\tau_c}, \\ I_c &= \frac{F}{4\pi}\sec\theta_r (p_c \varpi_c \tau_c) e^{-m\tau_{gc}}. \end{aligned} \tag{7}$$

Although we do not use these last approximations, they emphasize that thescattering properties of aerosol and cloud affect the radiance principally in the combinations

$$p_a \varpi_a \tau_a \qquad \text{and} \qquad p_c \varpi_c \tau_c,$$

so in practice not all the variables appearing in equations (4)–(6) are independent.

[13] Whereas the surface reflectance cancelled neatly from the ratios of radiances in equation (1), it is clear that such will not be the case when scattered radiance is taken into account. Nevertheless, equation (1) suggests the definition for any atmosphere of an apparent optical path difference (AOPD)

$$\ell_j = -m^{-1}\ln X_j. \tag{8}$$

In a clear atmosphere, ℓ_j is the difference between the optical thicknesses at frequencies ν_j and ν_0, and coincides with L_j. In a scattering atmosphere, ℓ_j depends on the reflectance, the scattering properties of the layers, the scattering geometry and the vertical distribution of the scattering material. However, the dependence on r in ℓ_j is much weaker than in the original radiances. The art of the analysis is to reduce the sensitivity of ℓ_j to r to such a level that the weaker dependence on the CO_2 column may be resolved. Clearly, the brighter the surface, the less sensitive is the total radiance to the scattered component, so differential absorption may be expected to provide accurate data when viewing bright targets, such as glint or bright land surfaces.

3.2. Surface Reflectance, Coverage, and Doppler Shifts

[14] Land surfaces generally are bright at 1.61 μm, while the oceans are dark except near glint. For example, images acquired on the nadir scan of the Along Track Scanning Radiometer (ATSR), extracted from the archive for the Australian region held at CSIRO Atmospheric Research, show that the albedo of land at 1.6 μm often exceeds 20%, but that for clear ocean water is typically only 0.3%. However, radiance reflected from the ocean has diffuse and specular components, the first consisting of photons reflected at the air-sea boundary, and the second of photons that have penetrated the water and subsequently escaped after being scattered by water molecules or hydrosols. The diffuse component (mostly observed by ATSR) is very low because water is strongly absorbing at 1.61 μm, but the specular component, which is less sensitive to the imaginary part of the refractive index, becomes large in the region of glint. Consequently, if it is important that the target be bright in order to minimize the errors caused by scattering in the atmosphere, it is natural to propose that observations over the oceans should be directed towards glint. However, this course of action raises two serious issues.

[15] First, observing glint will restrict the spatial coverage, thereby limiting the impact of the data upon mapping sources and sinks of CO_2. Indeed, when the low probability of clear pixels is taken into account, one may suspect that the coverage will be so limited that the data will have little impact, even if an accuracy of 0.5% can be achieved for individual measurements of CO_2 column.

[16] Second, because the relative velocity of satellite and glint can be large, particularly when the satellite is at high latitudes, Doppler shifts may be comparable (or even larger) than the spectral resolution of the observing instrument. In this case, it would be essential to compensate for Doppler shifts by tuning the frequency of the spectrometer dynamically. This facility is available with solid etalons fabricated from an electro-optic material, such as lithium-niobate. The refractive index of the etalon, and hence its passband, may be varied by applying a potential difference between the faces of the etalon.

[17] In addition, combinations of channels other than simple ratios (as in equation (1)) may be needed to cancel any residual shift caused by imperfect dynamical tuning of the spectrometer. For example, one method suggested by G. Toon (personal communication, 2000) is to use four channels symmetrically placed around an absorption line with two (A and D) in the far wings where absorption is weak and two (B and C) near the points of inflection of the absorption curve. The ratio $(B + C)/(A + D)$ should be immune to Doppler shifts.

3.3. Optical Properties of CO_2, O_2, and H_2O

[18] Even if precise estimates of the CO_2 column can be derived from observations of the optical path difference, the

accuracy of the estimates will depend upon the accuracy with which the spectroscopic properties of CO_2 are known. Of similar concern for O_2 at 1.27 μm are air glow and the continuum, which has components proportional to pressure and to pressure squared [*Smith and Newnham*, 2000]. While H_2O lines may be avoided in designing the instrumentation, the continuum of H_2O will be unavoidable, and its properties must be known precisely so that variations of the continuum across the spectral ranges of interest can be modeled. Furthermore, it was assumed that absorption features in the solar spectrum would cancel from ratios of radiances, but in practice solar lines will be Doppler shifted relative to atmospheric lines due to the earth's rotation and the ellipticity of the earth's orbit around the sun. Hence, if solar lines cannot be avoided, then they too must be modeled. It is an open question as to whether laboratory measurements can determine the line and continuum absorption of CO_2, O_2 and H_2O and their dependence on pressure and temperature with accuracy better than 0.5%. Thus it is likely that an extensive program of vicarious calibration would be required if measurement of CO_2 from space were to be made operational.

3.4. Temperature Sensitivity

[19] Although other satellite sensors measure the temperature profile, and meteorological models do their best to predict it, some uncertainty will remain. Thus the radiances measured in space will vary with the amount of CO_2 and with the temperature profile, so an uncertainty in either variable can mask changes in the other. It is imperative, therefore, to select frequencies where the sensitivity of the CO_2 absorption to temperature is minimized.

3.5. Spectral Resolution and SNR

[20] Because the absorption lines in the 1.61 μm band are relatively weak, the transmittance of the atmospheric column rises to near unity between the lines. Consequently, radiance measured at low spectral resolution (spanning many lines) will be dominated by the contributions from the near transparent regions between the lines. These contributions respond only weakly to changes in CO_2. In contrast, radiance measured with high spectral resolution will respond strongly to CO_2 if the measurement frequency lies on an absorption line. Thus high spectral resolution appears to be essential if small changes in CO_2 volume mixing ratio are to cause measurable changes in radiance. However, simultaneous attainment of high signal-to-noise ratio and high spectral resolution poses a serious technical challenge.

3.6. Data Assimilation

[21] Assuming that accurate measurements of the optical path difference L_j can be made from space, there still remains the task of analysis of such measurements in order to determine sources and sinks of CO_2. This is a formidable problem, which necessarily will involve modeling the diurnal and seasonal cycles of CO_2 production, as well as the mechanisms for transport of CO_2. How then might measurements of L_j be used?

[22] As a very first approximation, measurements of L_j may be interpreted as measurements of the CO_2 column, and may be binned to form daily and monthly averages. However, because the sampling will be biased, for example by satellite overpass times, cloud cover and seasonal changes, the same will apply to the averages.

[23] More ambitiously, measurements of L_j at several frequencies may be used to estimate not only the column amount but also the density profile of CO_2. Methods of Bayesian estimation, as described by *Rodgers* [2000] and applied to radiance measurements in the thermal infrared by *Engelen et al.* [2001], will be required. For measurements in the wings of spectral lines, the weighting functions, which describe the relative importance of contributions to the radiance from different heights in the atmosphere, decrease steadily with height. In contrast, weighting functions near line centers increase with height. Thus by using a judicious combination of both spectral regions, it may be possible to deduce a coarse vertical profile in addition to the CO_2 column.

[24] In the most ambitious approach, measurements of L_j at one or more frequencies may be assimilated directly by a chemical transport model in order to estimate sources and sinks of CO_2 using the techniques of synthesis inversion, as described by by *Enting et al.* [1995] and *Rayner et al.* [1999]. To do so, the surface pressure, temperature profile and specific absorption of CO_2 must be known in order to calculate L_j within the model. Used in this way, measurements of L_j from space provide constraints on the CO_2 density profile, rather than direct observations of the CO_2 column. Thus the chemical transport model provides a way of assimilating satellite data along with conventional measurements, such as flask samples.

[25] Given the complexity of the issues, it is likely that all three approaches will be needed, in addition to the complementary infrared measurements, which respond most strongly to CO_2 in a slab between 50–80 kPa [*Engelen et al.*, 2001].

4. Models of Instrument and Atmosphere

[26] We suppose that the radiometer measures at selected frequencies in the 1.61 μm absorption band of CO_2 and the 1.27 μm absorption band of O_2, sections of which are shown in the top panels of Figures 1 and 2. All spectra were computed using the line-by-line code GENLN2 [*Edwards*, 1992] and the HITRAN data base [*Rothman et al.*, 1992]. The 1.61 μm band was chosen because, in contrast with other candidate bands at 1.4 μm and 2.0 μm, it contains few water vapor lines, thus permitting absorption by water vapor to be represented in the vicinity of CO_2 lines by a smooth continuum. Furthermore, we suppose that the measurements are made at frequencies where the sensitivity of the atmospheric transmittance to temperature is minimized. As shown in the lower panel of Figure 1, the sensitivity to temperature passes through zero near the center of the P-branch, so we focus on absorption lines near 6210 cm^{-1}. Examination of the solar spectrum reveals strong lines at 6208.5 cm^{-1} and 6211.5 cm^{-1} (the latter due to Si), so we select the CO_2 line at 6205.339 cm^{-1}. Sensitivity to temperature passes through zero in the 1.27 μm band of O_2 near 7850 cm^{-1}, and in this case we select the line at 7855.131 cm^{-1}. We assume that the observations are made at high spectral resolution (full width at half height $\Delta\nu$ = 0.02 cm^{-1}) to ensure adequate sensitivity to changes in CO_2 column in the 1.61 μm band,

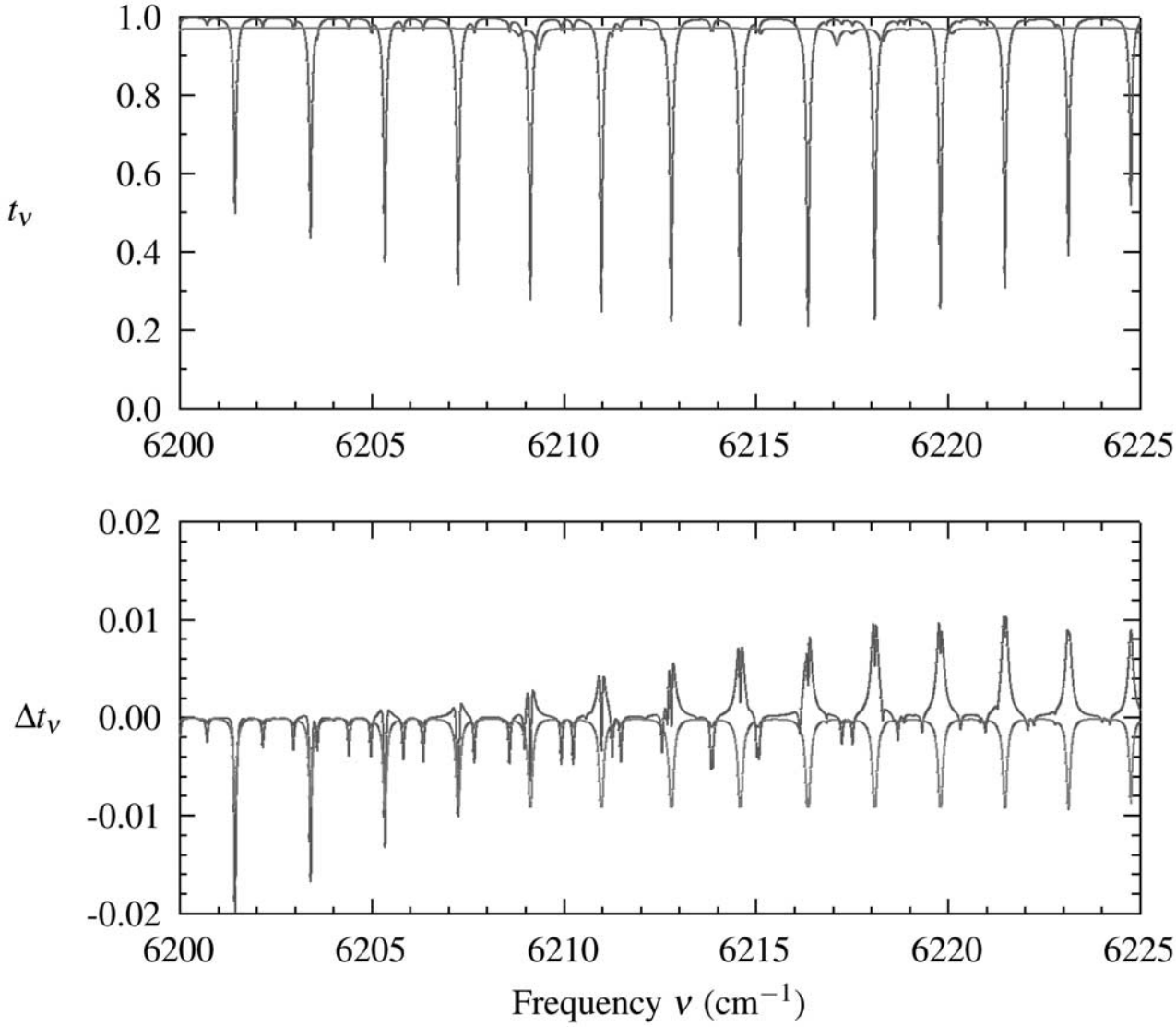

Figure 1. The top panel shows transmittance spectra from the surface to space of CO_2 (blue) and H_2O (red) in a section of the 1.61 μm band of CO_2. The blue curve in the bottom panel shows the change Δt_ν in the CO_2 transmittance caused by a 10 K increase in the temperature profile at all levels, whereas the red curve shows the change caused by an increase in the CO_2 concentration by 10 ppmv. Solar features are not included in the spectra.

and to avoid air glow in the 1.27 μm band. The transfer function of the radiometer is represented by a Gaussian, normalized so that its integral is equal to unity. Although these specifications may sound restrictive, most of the argument that follows may be applied elsewhere in the near infrared spectrum of CO_2.

[27] The radiometer is assumed to be calibrated, because the absolute radiance is a useful indicator of cloud in the field of view and provides an approximate value of the surface reflectance. However, the accuracy required of the calibration is not high, with an error of ±10% being acceptable, because analysis of the radiances will begin with the formation of ratios as in equation (1), a step that eliminates the dependence upon absolute calibration.

[28] The scattering properties of ice clouds are particularly important for the analysis. If the particles are assumed to be pure ice spheres, then the scattering phase function is small over the midrange of scattering angles that commonly occur in passive remote sensing. Such a model leads to an unrealistically optimistic assessment of the error in measurements of CO_2, because the scattered radiance is depressed. Ice crystals in the form of hexagonal cylinders, modeled for example by *Takano and Liou* [1989], would be more realistic, because they exhibit halos at 22° and 46°. However, real ice clouds are even more complex, containing many crystalline habits, often with surfaces that are not the smooth planes of the ideal hexagonal model, but rather are roughened or rimed. For such clouds, more radiance is scattered at the midrange angles, and therefore the asymmetry parameter of the scattering phase function is smaller. For example, *Gerber et al.* [2000] and *Garrett et al.* [2000] report on measurements in arctic ice clouds with a cloud integrating nephelometer, in which they found asymmetry parameters as low as 0.74 at visible wavelengths. For this

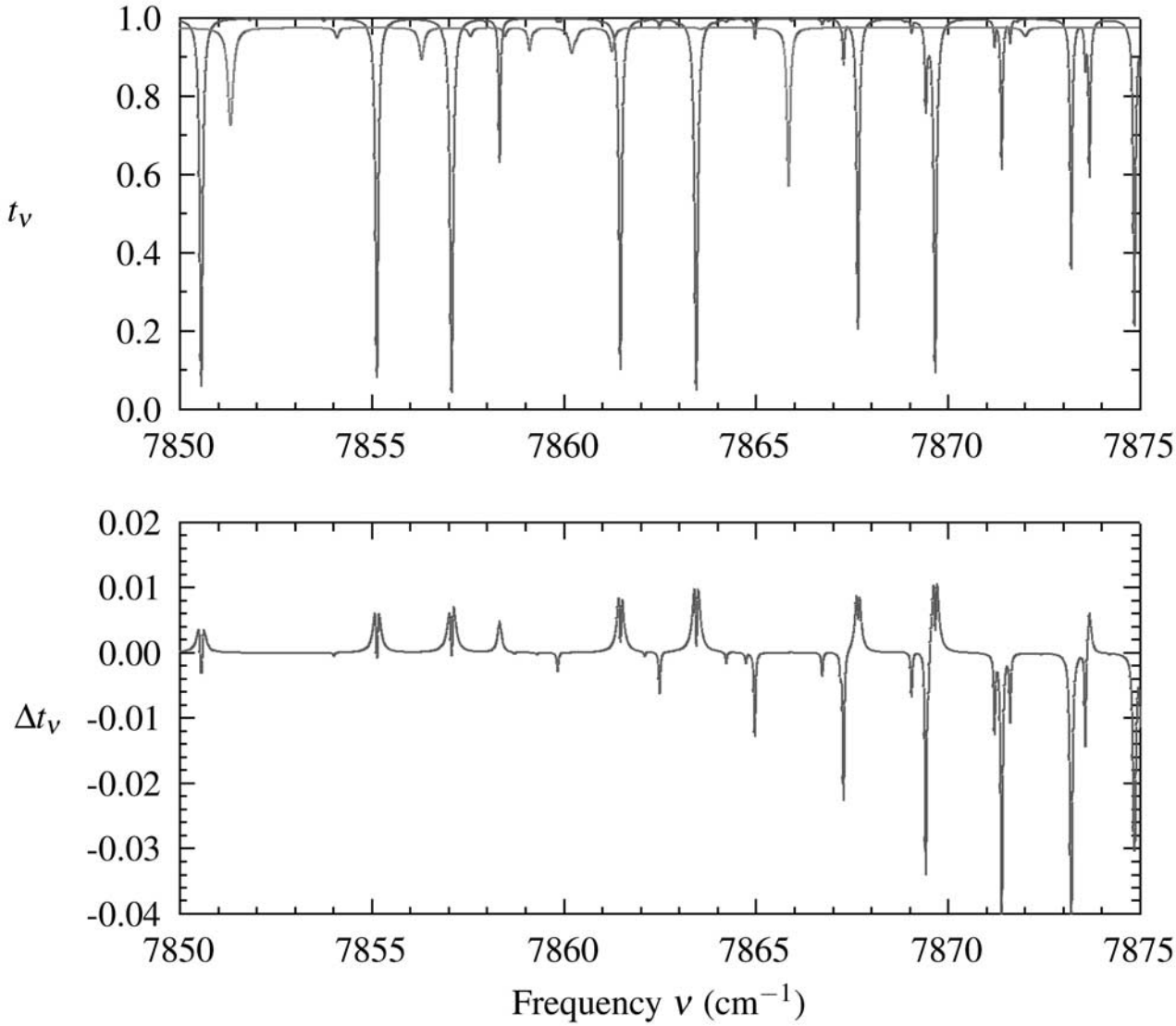

Figure 2. The top panel shows transmittance spectra from the surface to space of O_2 (blue) and H_2O (red) in a section of the 1.27 μm band of O_2. The bottom panel shows the change Δt_ν in the O_2 transmittance caused by a 10 K increase in the temperature profile at all levels. Solar features are not included in the spectra.

paper it is imperative that the effects of cirrus not be underestimated, so we have taken the simple phase function proposed by *Henyey and Greenstein* [1941] with asymmetry parameter in the range 0.75–0.85 to represent scattering by ice clouds. While *Fu and Takano* [1994] correctly point to the inadequacy of the Henyey-Greenstein phase function for representing the complex scattering by ice clouds consisting of hexagonal cylinders, we use the Henyey-Greenstein phase function simply to provide a realistic upper bound to the scattered radiance, and hence to provide a conservative estimate of the consequent error in the CO_2 column. In the same sense, we also use a Henyey-Greenstein phase function to represent scattering by aerosol.

[29] Although the dependence on frequency ν is not shown explicitly in equations (4)–(6), the gas transmittances and optical thicknesses are strong functions of frequency. In contrast, the optical properties of the scatterers are assumed to be constant across the CO_2 channels and across the O_2 channels, but variation between the CO_2 and O_2 channels may be important. In this paper we assume that the variation may be predicted reliably on the basis of microphysical properties, but we flag it as an issue for future investigation.

[30] Anticipating that accurate measurement of CO_2 requires a bright surface, we assume for the reflectance the model of glint developed by *Cox and Munk* [1954] for a rough sea surface. *Cox and Munk* [1954] observed that the glint is caused by specular reflection from the myriad of facets on the surface of the sea that are inclined at the correct angle to reflect sunlight directly to the observer, the distribution of which is approximately Gaussian with variance σ^2 linearly related to wind speed v,

$$\sigma^2 = av + b, \; a = 0.00512, \; b = 0.003 \text{ and } v \text{ in m s}^{-1}.$$

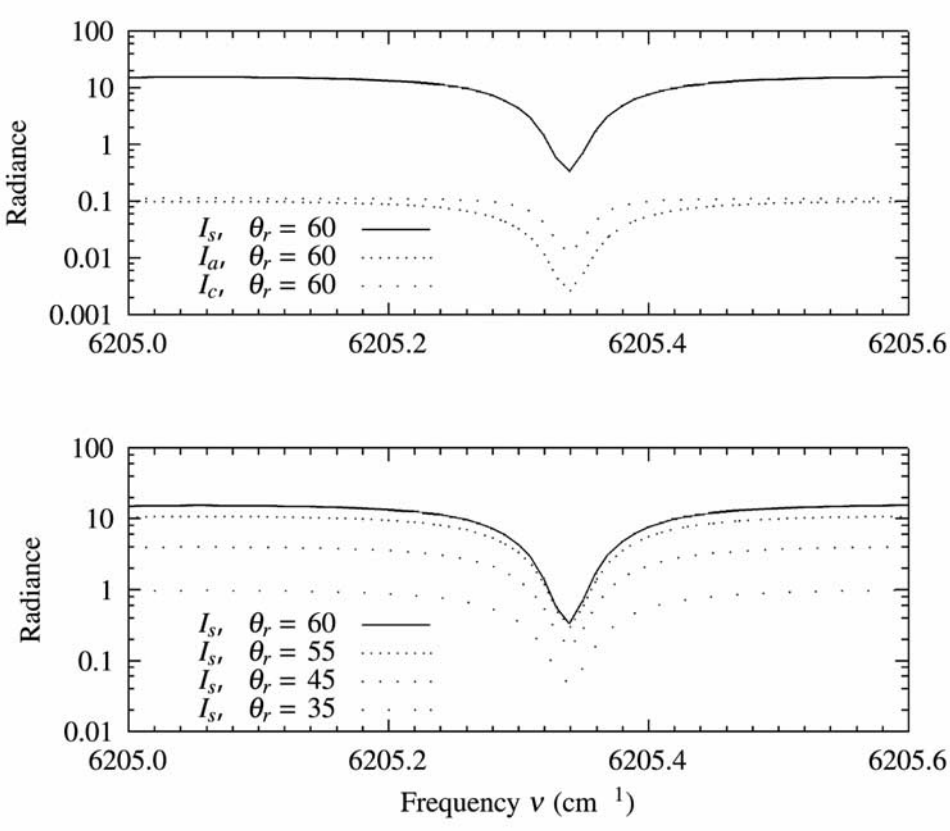

Figure 3. The top panel shows the radiance components reflected from the surface (I_s), scattered by aerosol (I_a), and scattered by thin cloud (I_c). The units of the radiance are mW m^{-2} sr^{-1}. The bottom panel shows the surface component when the view zenith (θ_r) moves away from the specular point at 60° to 35°. In each case the scattering is in the plane containing the Sun, the satellite and the specular point.

The reflectance has the form

$$r = \sigma^{-2}\sec^4\chi\exp\left(-\sigma^{-2}\tan^2\chi\right)R(i,n), \qquad (9)$$

where χ is the angle between the vertical and the normal to the plane so inclined that the incident beam from the sun is reflected specularly to the observer, i is the angle of incidence of the solar beam onto that plane, and R denotes Fresnel's reflection coefficient. The last depends upon the frequency of the radiation and the refractive index n of sea water at that frequency.

[31] In addition to the glint, the sea also reflects sunlight diffusely, principally from scattering by hydrosols and white caps. These components, which typically give ocean albedos less than 0.5% at 1.6 μm, are not included in the model of equation (9). However, they are not relevant to this study because the reflectance must be high, if the CO_2 column is to be measured accurately, and this requires glint, which conforms to equation (9).

[32] Figure 3 shows the components I_s, I_a and I_c averaged over a transfer function with resolution $\Delta\nu = 0.02$ cm^{-1} in the vicinity of the CO_2 absorption line at 6205.339 cm^{-1}. The thermodynamic profile of the atmosphere is assumed to be that of the midlatitude summer atmosphere [*McClatchey et al.*, 1972], and the CO_2 volume mixing ratio is assumed to be 380 ppmv. The scattering is in the principal plane with zenith angles of incidence and reflection $\theta_i = 120°$ and $\theta_r = 60°$, so the scattering angle is $\psi = 60°$ and the airmass is $m = 4$. The wind speed is assumed to be 5 m s^{-1}, leading to reflectance $r = 1.98$ predicted by equation (9). The cloud is assumed to be located at height $z_c = 8.5$ km and to have optical thickness $\tau_c = 0.02$, asymmetry parameter $g_c = 0.75$ and single scattering albedo $\varpi_c = 1$. Similarly, the aerosol is at height $z_a = 1.1$ km with $\tau_a = 0.02$, $g_a = 0.75$ and $\varpi_a = 1$. The optical thickness for aerosol is close to the detectable limit, whereas thinner cloud may be detected because it is higher. Nevertheless, these conditions are very clear. Figure 3 shows that the scattered components of the radiance are at least a factor of 100 smaller that the component reflected from the surface. However, the reflected radiance falls rapidly when the view zenith angle θ_r moves away from the center of the glint; at $\theta_r = 35°$, the reflected component of the radiance is only ten times larger than the scattered components.

[33] The sensitivity of AOPD ℓ_j to variable x (for example, u, T, r, τ_a or τ_c) is represented by

$$\frac{1}{\ell_j}\frac{\partial \ell_j}{\partial x}.$$

For variables such as r, τ_a and τ_c that appear explicitly in the model, the calculation of the corresponding sensitivities is straightforward. The sensitivity of ℓ_j to CO_2 column was calculated by numerical differentiation of the transmittance

after convolution with the transfer function of the spectrometer. The sensitivity of ℓ_j to temperature was estimated similarly by displacing the temperature profile uniformly from the MLS profile. This procedure is likely to lead to an overestimate of the sensitivity to temperature errors, because errors at different heights usually will be weakly correlated. Nevertheless, in the present application conservative estimates of accuracy are preferable. The sensitivity of ℓ_j to each of u, r, τ_a and τ_c varies slowly with frequency, whereas the sensitivity to T changes sign across the absorption band.

[34] In addition to the apparent optical depth defined in equation (8), we also define δ_j, the reduction in AOPD arising from scattering in the atmosphere, by

$$\delta_j = \ell_j^\star - \ell_j,$$

where $\ell_j^\star$ denotes a fixed reference value for the AOPD. For CO_2, we take $\ell_j^\star$ to be the optical thickness in a clear atmosphere with 380 ppmv of CO_2. In principle, δ_j may be either positive or negative.

5. Error Analysis

5.1. Simplified Analysis

[35] Using the sensitivity of AOPD to u, r, T, τ_c and τ_a, we can estimate very simply the uncertainty in u arising from uncertainties in r, T, τ_c and τ_a. Uncertainties caused by the heights of the scattering layers, their scattering properties and the scattering geometry will be examined later. If two atmospheric states differ by amounts Δu, Δr, ΔT, $\Delta\tau_a$, $\Delta\tau_c$, then the corresponding AOPDs in channel j will differ by

$$\Delta\ell_j = \frac{\partial\ell_j}{\partial u}\Delta u + \frac{\partial\ell_j}{\partial r}\Delta r + \frac{\partial\ell_j}{\partial T}\Delta T + \frac{\partial\ell_j}{\partial\tau_c}\Delta\tau_c.$$

However, if the differences are related so that

$$\Delta\ell_j = 0,$$

then the measured AOPDs will be identical, and uncertainty in one variable will mask that in another. For example, if the states differ only in u and τ_c and

$$\Delta u = -\frac{\partial\ell_j/\partial\tau_c}{\partial\ell_j/\partial u}\Delta\tau_c, \tag{10}$$

then the radiances reflected to space will be the same for the two atmospheric states, and the difference $\Delta\tau_c$ will mask from the observer a difference Δu, and vice-versa. Thus Δu given by equation (10) is a measure of the uncertainty in u caused by an uncertainty $\Delta\tau_c$. Similar arguments apply to the other variables. If typical values are specified for the uncertainties in r, T, τ_a and τ_c, then equation (10) and its analogues allow the corresponding errors induced in u to be estimated.

[36] Table 1 shows the results of such a calculation. First, temperature errors appear to be secondary, especially so because the estimates in Table 1 are based on an assumed bias in the temperature profile of 1 K at all levels, rather than errors that are weakly correlated at different levels. Thus with global data from infrared sounders, the Advanced Microwave Sounding Unit (AMSU) and GPS occultations, the accuracy of the temperature field produced by numerical weather prediction models should be adequate. Second, errors in r do not appear be a limiting factor over bright surfaces, because a calibrated measurement of the radiance in any one of the frequency channels should fix r within the tolerance of 0.2 assumed in Table 1. Third, the most serious errors in u are caused by undetected clouds. Although it may be possible to detect thin cloud using (for example) radiances in the O_2 A-band [*Heidinger and Stephens*, 1998], Table 1 shows that the errors in the CO_2 column are unacceptably large, even when the optical thickness of undetected cloud is as low as $\tau_c = 0.02$. It seems extremely unlikely, therefore, that CO_2 column can be inferred reliably from measurements in CO_2 absorption bands alone. Consequently, additional independent measurements and more sophisticated analysis will be required to diagnose cloud and to compensate for the radiance it scatters. In the next section, we explore the impact of adding observations in an O_2 absorption band.

Table 1. Percentage Errors ($\Delta u/u$) in CO_2 Column u Caused by Errors ΔT, Δr, $\Delta\tau_c$ and $\Delta\tau_a$ for Three Values of the View Zenith Angle θ_r

	θ_r		
	60°	50°	40°
r	1.98	1.11	0.39
$\Delta T = 1$ K	−0.25	−0.25	−0.25
$\Delta r = 0.2$	−0.10	−0.22	−1.19
$\Delta\tau_c = 0.02$	0.91	1.06	2.07
$\Delta\tau_a = 0.02$	0.23	0.26	0.49

5.2. Analysis With Both CO_2 and O_2 Channels

5.2.1. Correlation Between CO_2 and O_2 Channels

[37] The reason why high cloud introduces such a large error is easily understood: photons scattered to space from high in the atmosphere do not traverse the full column of CO_2, and hence suffer less absorption, leading to an underestimate of the amount of CO_2. In order to reduce the error, the AOPD for CO_2 may be compared with that for O_2 in a channel with a similar column transmittance. Because the ensembles of photon trajectories will be similar, the radiances in the two channels should be tightly correlated, even in the presence of scattering, thereby allowing the CO_2 column to be determined relative to that of O_2. The latter may be deduced from surface pressure, because O_2 is well mixed and its volume mixing ratio does not show day-to-day variations on the same scale as CO_2. The World Meteorological Organization (WMO) requirement for pressure fields is an accuracy of 0.05% [*World Meteorological Organization* (*WMO*), 1993]. While weather forecast models may not achieve this accuracy yet, there is every reason to believe that in the next few years an accuracy of 0.5% will be obtained routinely as more accurate temperature profiles become available from advanced infrared sensors and analysis of occultation of GPS signals.

[38] To test these ideas, radiances were simulated for the frequencies shown in Table 2. The CO_2 frequencies were

Table 2. Frequencies Used in the Simulations[a]

j	CO_2, cm^{-1}		O_2, cm^{-1}		
	ν	t_ν	ν	t_ν	I_{ag}/I_s
0	6204.500	0.99	7854.500	1.00	≈0
1	6205.296	0.74	7855.060	0.75	4.0×10^{-8}
2			7855.080	0.62	2.8×10^{-3}

[a] The CO_2 frequencies were chosen to minimize absorption by water vapor and sensitivity to temperature. The first two O_2 frequencies were selected to match the column transmittance (t_ν) in the corresponding CO_2 channels. The last column gives the air glow radiance as a fraction of the radiance reflected from a surface with $r = 0.1$.

selected to minimize temperature sensitivity, while those for the first two O_2 channels were chosen from the 1.27 μm absorption band to match the optical depths in the corresponding CO_2 channels. While the 1.27 μm band of O_2 is the closest O_2 band (with significant absorption) to the CO_2 1.61 μm band, thereby minimizing the differences in scattering properties of aerosol and cloud between the two wavelengths, the 1.27 μm band is noted for its air glow emission, which could pose a serious practical problem. Fortunately, that emission is concentrated in the centers of the lines with Doppler widths of approximately 0.01 cm^{-1}, because most of the emission originates above 70 km as excited O_2 states are quenched by collisions at lower altitudes [*Noxon*, 1982]. Therefore, the air glow contribution to the radiometer channels will be small if the channels are narrow and avoid the line centers.

[39] *Noxon* [1982] states that the total air glow radiance integrated over the 1.27 μm band is $I_\star = 3 \times 10^{17}$ photons $m^{-2}\,s^{-1}\,sr^{-1}$. This emission is produced in $n \approx 100$ spectral lines, each with Doppler width $\alpha_\star \approx 0.01$ cm^{-1}. Assuming that the emission is isotropic and that the lines contribute approximately equally to the total, the convolution of the air glow radiance emitted to space with a Gaussian filter representing the transfer function of the spectrometer yields for the detected air glow radiance

$$I_{ag} = \sec\theta_r \frac{I_\star}{n\sqrt{\pi}\alpha} \exp\left[-\left(\nu_\star - \nu_j\right)^2/\alpha^2\right].$$

In this expression, $\nu_\star$ is the central frequency of the air glow line, ν_j is the central frequency of the instrument transfer function, and

$$\alpha = \sqrt{\alpha_\star^2 + \alpha_j^2},$$

where α_j is related to $\Delta\nu$, the full width at half height, of the transfer function by

$$\alpha_j = \Delta\nu/\left(2\sqrt{\ln 2}\right).$$

The last column of Table 2 represents the air glow contribution to the radiance as a fraction of the radiance reflected from the darkest ($r = 0.1$) surface considered in this paper. For the channels at frequencies ν_0 and ν_1, the air glow is negligible. While there is a small contribution at ν_2, we will see later that this channel is used only to estimate cloud height, a noncritical function.

[40] For every geometrical and scattering combination shown in Table 3, the surface reflectance, the radiances and the AOPDs were computed for each of the O_2 and CO_2 channels. The calculations were repeated for different CO_2 column amounts with $\Delta u/u$ in the range 0–4%. The tightness of the correlation between $\delta_1(O_2)$ and $\delta_1(CO_2)$ is illustrated in Figure 4, which is a scatter plot color-coded to show points with $\Delta u/u$ = 0%, 2% and 4%. Because scatterers reduce the average photon path length, which in turn reduces the AOPD by more than the optical thickness of the scatterers, $\delta_1(O_2)$ is low for clear atmospheres and increases with the amount of scattering material. Despite the large variations in both $\delta_1(CO_2)$ and $\delta_1(O_2)$, in each case considerably larger than the changes caused by the different CO_2 columns, they remain well correlated throughout. However, it is important to emphasize that the tight correlation evident in Figure 4 requires that the absorption profiles of CO_2 and O_2 be matched closely to ensure that the photons follow similar trajectories. Simulations (not reproduced here) with two O_2 lines, similar in strength but differing in their sensitivities to pressure and temperature, show that the line whose absorption profile more closely matches that of the CO_2 line leads to the tighter correlation.

[41] When the cloud is located at level i, the correlation between $\delta_1(O_2)$ and $\delta_1(CO_2)$ may be parameterized in the form

$$\delta_1(CO_2) = h_i(\delta_1(O_2), \Delta u), \tag{11}$$

Table 3. Parameter Values Used in the Simulations Involving Both CO_2 and O_2 Channels

Parameter	Symbol	Minimum	Maximum	Increment	Steps
Incident zenith angle	θ_i	120°	170°	5°	11
Incident azimuth angle	ϕ_i	0°	0°	0°	1
Reflected zenith angle	θ_r	10°	70°	5°	13
Reflected azimuth angle	ϕ_r	0°	0°	0°	1
Surface wind speed, m s^{-1}	ν	5	5	0	1
Aerosol optical thickness	τ_a	0	0.2	0.02	11
Aerosol asymmetry parameter	g_a	0.75	0.75	0	1
Aerosol single scattering albedo	ϖ_a	1	1	0	1
Cloud optical thickness	τ_a	0	0.1	0.02	6
Cloud asymmetry parameter	g_c	0.75	0.75	0	1
Cloud single scattering albedo	ϖ_c	1	1	0	1
Change in CO_2 column, %	$\Delta u/u$	0	4	0.4	11

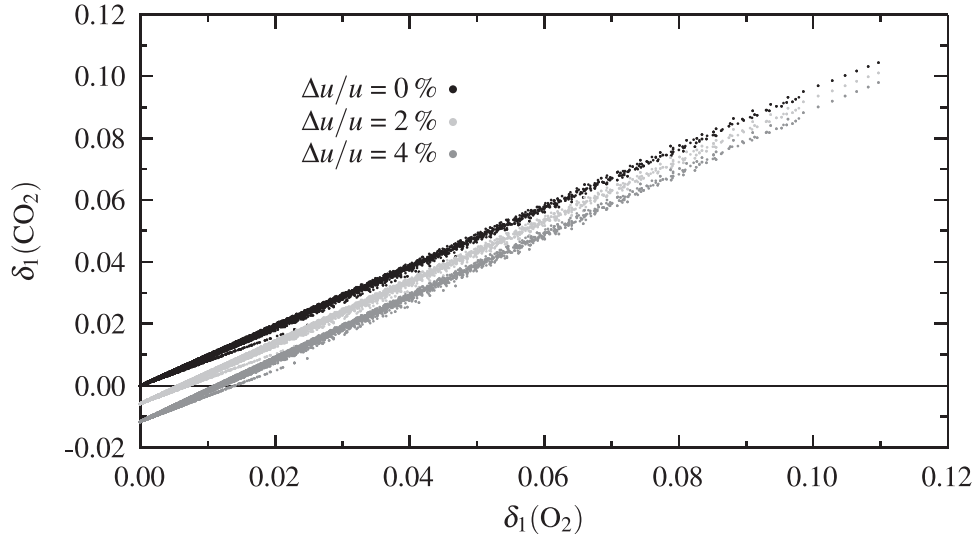

Figure 4. Correlation between $\delta_1(O_2)$ and $\delta_1(CO_2)$ for the simulations specified in Table 3. The three clusters of points (from top to bottom) correspond to CO_2 column amounts differing from the reference by 0%, 2% and 4%.

where

$$h_i(x,y) = f_i(g_i(x,y)), \qquad g_i(x,y) = m_i(y)x + n_i(y), \qquad (12)$$

and f_i, m_i and n_i are low order polynomials and x and y are dummy arguments. We chose polynomials with degree 3, and determined the coefficients using nonlinear least squares analysis.

5.2.2. Effect of Scattering Properties

[42] The tightly correlated AOPDs for CO_2 and O_2 in Figure 4 were obtained with varying optical thicknesses for aerosol and cloud, but fixed values for the asymmetry parameters and single scattering albedos. However, as shown in equation (7), the latter variables appear in the (approximate) representations of the scattered radiance in the combinations $p_a\varpi_a\tau_a$ and $p_c\varpi_c\tau_c$, so we anticipate that varying the scattering properties will not have a large effect upon the correlation between the AOPDs for CO_2 and O_2. Indeed this is the case, as shown by calculations (omitted) with values of 0.75 and 0.85 for the asymmetry parameters of both aerosol and cloud. Although more photons are scattered to the satellite sensor with the lower value of the asymmetry parameter, leading to wider ranges for $\delta_1(CO_2)$ and $\delta_1(O_2)$, the correlation between $\delta_1(CO_2)$ and $\delta_1(O_2)$ is

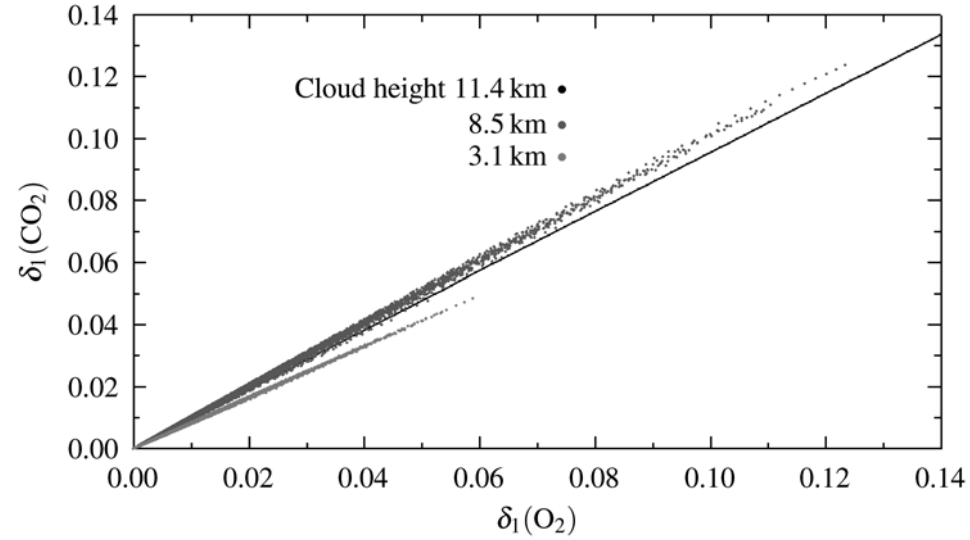

Figure 5. The middle line is the parameterized correlation with cirrus cloud at height 8.5 km. The upper and lower clusters of dots are data computed with cirrus cloud at heights 11.4 km and 3.1 km, respectively. For all three data sets, the CO_2 column amount is fixed at the reference value. Other parameters for the simulations are specified in Table 3.

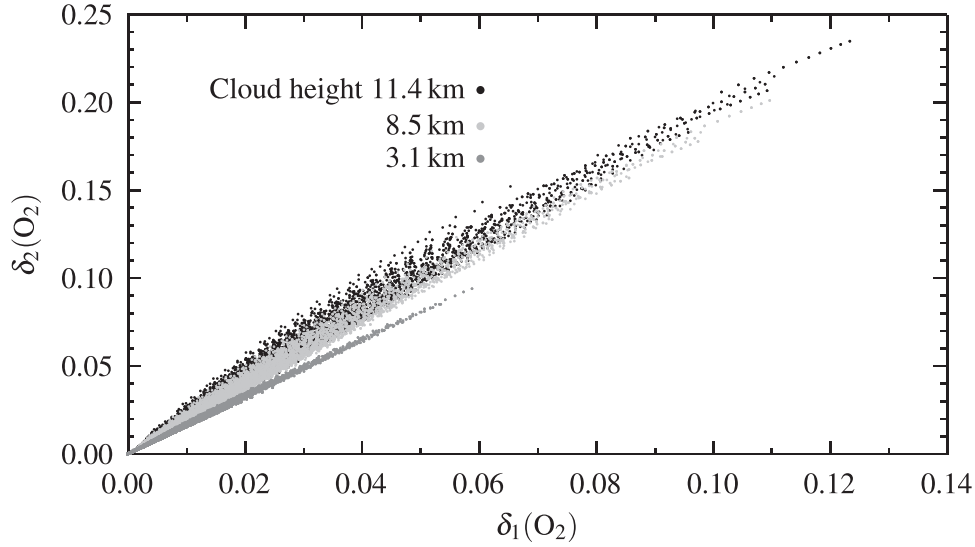

Figure 6. Correlation between $\delta_1(O_2)$ and $\delta_2(O_2)$ for the simulations specified in Table 3. The three clusters of points correspond to cirrus cloud at heights 11.4, 8.5 and 3.1 km.

almost unchanged, simply because photons in the CO_2 and O_2 channels follow similar trajectories.

5.2.3. Effect of Cloud Height

[43] In contrast to the scattering properties, cloud height has a marked impact upon the correlation between $\delta_1(CO_2)$ and $\delta_1(O_2)$. The solid curve in Figure 5 represents the function h_{15} for cloud at height 8.5 km (level 15) and the reference CO_2 column. The upper and lower clusters of dots show the correlations for clouds at heights 11.4 km and 3.1 km, in each case with the same CO_2 column. While the correlation remains tight for each cloud level, the functional forms differ, and obviously will be a source of error if the cloud height is unknown. For example, if the cloud is actually at 11.4 km but the analysis assumes 5.8 km, then the error in the estimated CO_2 column could be as large as 4%. Perhaps more importantly, this error would be systematic.

[44] In order to determine the effective height of scattering, independent data are required. Ideally a bore-sighted lidar would be used to profile the scattering properties of the atmosphere, but a lidar would add considerably to the cost and complexity of a satellite mission. Here we assume that radiances are measured in three O_2 channels with frequencies indicated in Table 2.

[45] The AOPDs for the O_2 channels are not as tightly correlated as those for the CO_2 and O_2, because the O_2 channels have different absorption profiles, and therefore respond to scattering at different levels. Thus the correlations in Figure 6 between $\delta_2(O_2)$ and $\delta_1(O_2)$ for clouds at three levels are strong, but clearly overlap when the scatter-

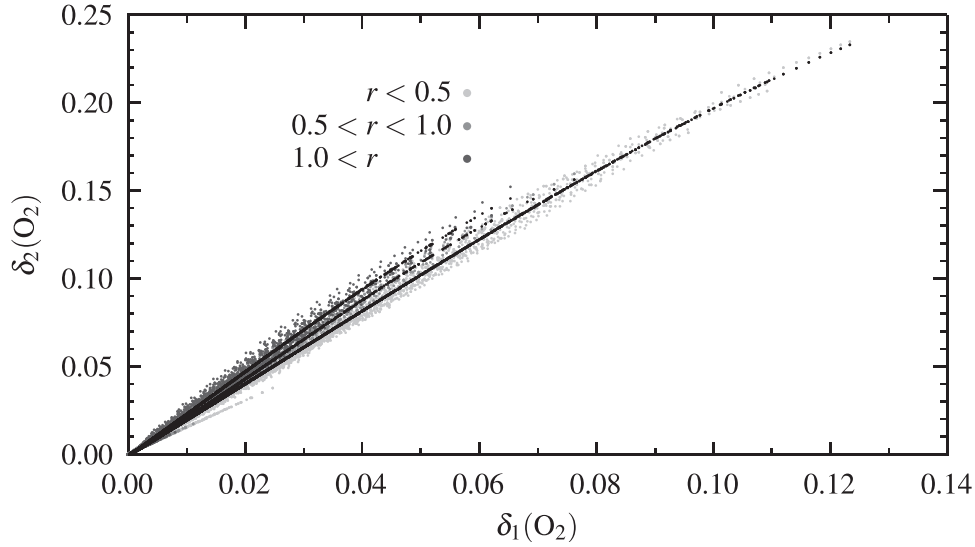

Figure 7. Stratification of the correlation between $\delta_1(O_2)$ and $\delta_2(O_2)$ according to surface reflectance r. The blue, red and green points correspond to cases with reflectance r in the bins $(0, \frac{1}{2})$, $(\frac{1}{2}, 1)$ and $(1, \infty)$. The black curves are parameterizations of the data points for the three bins. The cloud is assumed to be located at height 11.4 km.

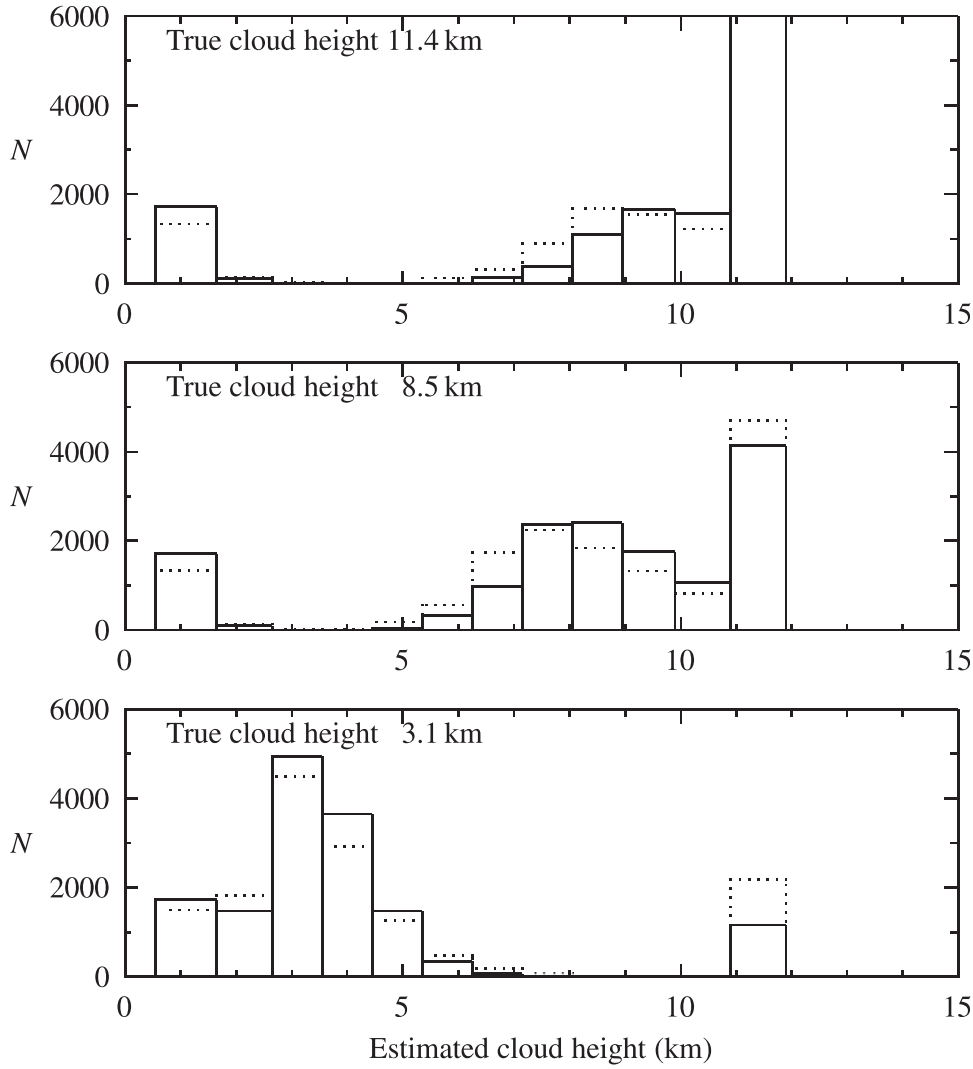

Figure 8. Histograms of cloud levels inferred from the O_2 channels. The true heights of the cloud layers for the panels were 11.4 km, 8.5 km and 3.1 km, respectively. The solid histograms were obtained using stratification of the reflectance, while the dotted histograms did not employ this device.

ing optical thickness is low. Furthermore, because the channel with lower O_2 optical thickness responds more strongly to surface reflectance, the correlation is stratified with respect to r. Figure 7 illustrates this point. Data are color-coded according to reflectance in three bins,

$$0 < r < \frac{1}{2}, \qquad \frac{1}{2} < r < 1 \qquad \text{and} \qquad 1 < r.$$

The points may be parameterized by functional forms similar to those used to parameterize the CO_2-O_2 correlation: for data in reflectance bin k and level l,

$$\delta_2(O_2) = H_k(\delta_1(O_2), l), \tag{13}$$

where

$$H_k(x,l) = F_k(G_k(x,l)), \qquad G_k(x,l) = M_k(l)x + N_k(l), \tag{14}$$

and F_k, M_k and N_k are low order polynomials and x is a dummy argument. Again, we used polynomials with degree 3 and determined the coefficients by nonlinear least squares analysis.

[46] Given a measurement $(\delta_1(O_2), \delta_2(O_2))$, the level l may be estimated by solving equation (13) by bisection with preset upper and lower limits for the cloud height. Histograms of cloud height so obtained are shown for clouds at heights 11.4, 8.5 and 3.1 km in Figure 8. Because the clouds were constrained by the algorithm to lie between the surface and 11.4 km, the relatively large numbers at these levels include situations where the data were inconsistent with the model underlying the algorithm. Each panel in Figure 8 contains two histograms. The first, obtained using functions F, M and N determined from all $(\delta_1(O_2), \delta_2(O_2))$ points without stratification according to reflectance, generally is inferior to that obtained using stratified functions F_k, M_k and N_k as defined above. Although the assignment of cloud height is approximate, as expected from the overlap of the clusters in Figure 6, we will see in the next section that the estimate of cloud height reduces both the bias and the variance of the errors in the estimates of the CO_2 column.

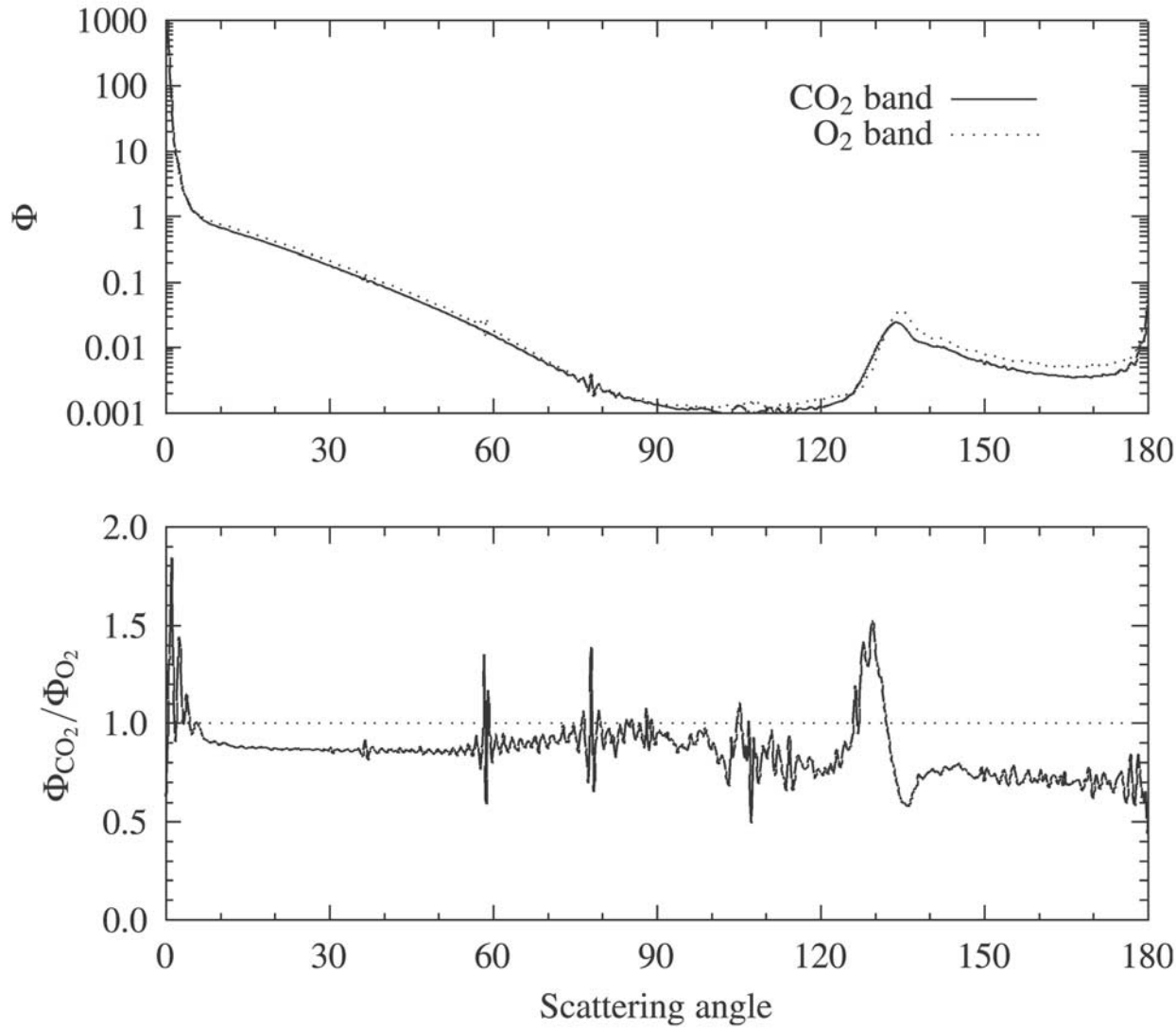

Figure 9. The top panel shows the scattering functions ($\times 10^8$) for ice spheres at wavelengths of 1.27 μm and 1.61 μm. The radii of the spheres are drawn from a power law distribution with effective radius 50 μm and effective variance 0.1. The bottom panel shows the ratio of the scattering functions.

5.2.4. Caveats

[47] There are three important provisos on these simulations, each of which requires careful investigation.

[48] First, the only variation in reflection coefficient between the CO_2 and O_2 channels was assumed to be caused by the change in the Fresnel reflection coefficient of bulk water. This assumption should be acceptable, provided that dissolved matter in the water does not have absorption bands at the wavelengths of 1.27 μm and 1.61 μm.

[49] Second, the scattering function Φ of the cirrus layer, defined for scattering angle ψ as the product of the scattering coefficient β and phase function p by

$$\Phi(\psi) = \beta p(\psi),$$

was assumed to be unchanged between 1.27 μm and 1.61 μm. This will not be the case in practice. However, for ice spheres, the differences between the scattering functions at the two wavelengths are small, as shown in the upper panel of Figure 9 computed for polydispersions of spheres whose radii were drawn from a power law distribution with effective radius equal to 50 μm and effective variance 0.1, the latter defined by *Mischenko and Travis* [1994]. Table 4 lists the key optical properties of the ice spheres. In these calculations, data for the refractive index of ice were drawn

Table 4. Scattering Properties of Ensembles of Ice Spheres Whose Radii Are Drawn From a Power Law Distribution With Effective Radius of 50 μm and Effective Variance 0.1

Quantity	Wavelength	
	1.27 μm	1.61 μm
Scattering coefficient ($\times 10^7$)	0.1192	0.1111
Extinction coefficient ($\times 10^7$)	0.1199	0.1203
Single scattering albedo	0.9943	0.9230
Asymmetry	0.8872	0.8999

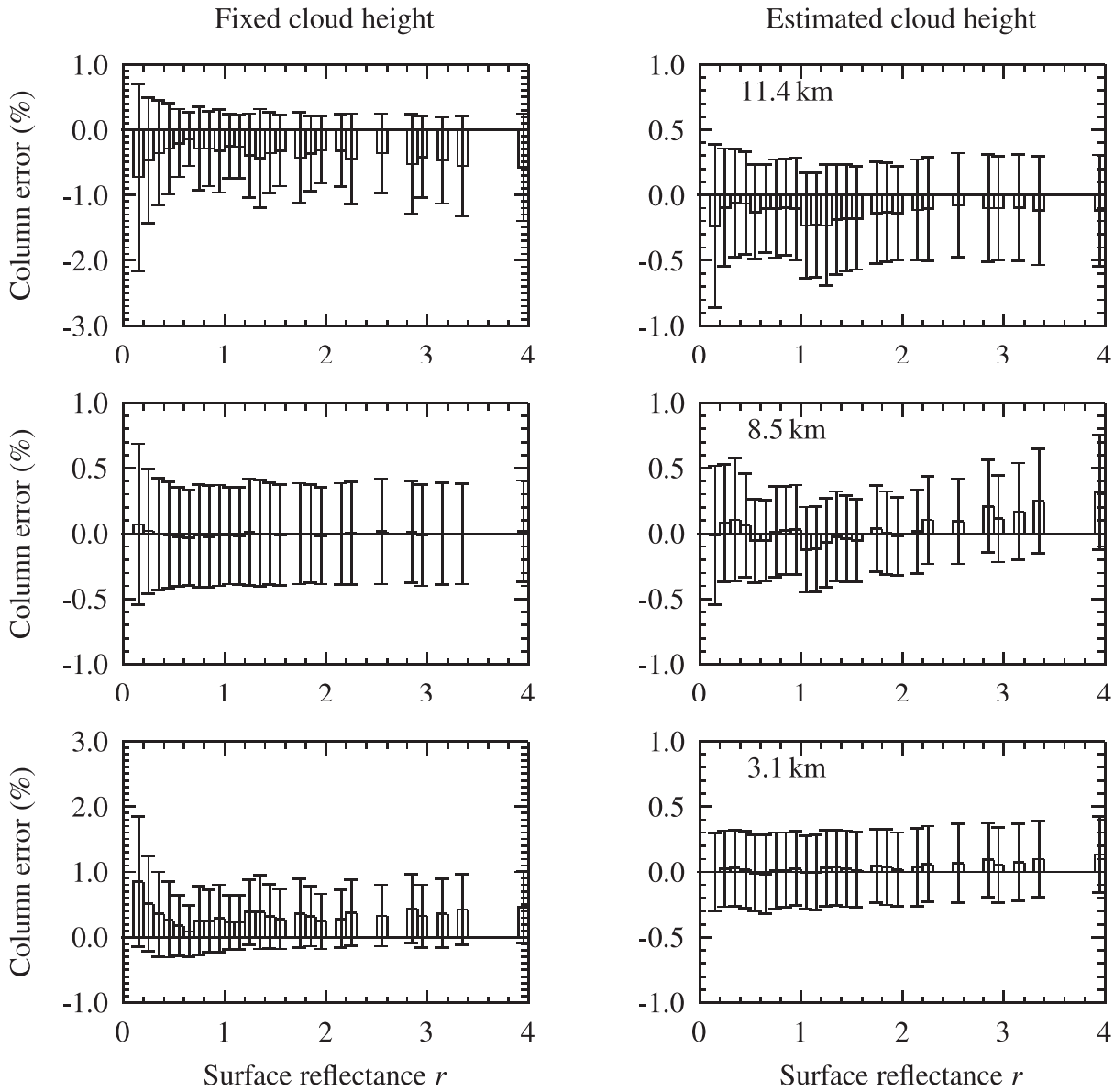

Figure 10. Percentage error in the estimated CO_2 column plotted as a function of the surface reflectance r. The rows from top to bottom correspond to clouds at levels 11.4 km, 8.5 km and 3.1 km. The analysis used for the left-hand column assumed cloud height fixed at 8.5 km, whereas cloud height was estimated from O_2 channels for the analysis on the right. The error bars indicate the standard deviation from the mean.

from *Warren* [1984], while the Mie calculations were carried out using the code published by *Wiscombe* [2000]. Although the differences between the scattering functions are small, they are important, because the ratio of the scattering functions is not unity, as shown in the lower panel of Figure 9. For ice spheres the ratio is predictable, and hence could be accommodated within the analysis, but whether a stable relationship exists between the scattering functions for more realistic models of ice crystals is an open question.

[50] Third, the modeling has assumed that O_2 and CO_2 are uniformly mixed throughout the atmosphere. While this is a good approximation for O_2, significant vertical gradients exist in the CO_2 volume mixing ratio, particularly near the surface. Such gradients, which vary with time of day, season and environmental conditions, will affect the correlation between O_2 and CO_2 AOPDs. The impact of such variations is unknown at present.

6. Inversion Algorithm and Error Statistics

[51] The parameterized curves defined by equations (11) and (12) depend principally upon the absorption characteristics of CO_2 and O_2, and only secondarily upon the scattering properties of the atmosphere. Thus Δu may be estimated from $(\delta_1(O_2), \delta_1(CO_2))$ by solving equation (11), provided that the cloud height is known. In practice the height may be assumed or may be estimated from the O_2 channels. When radiances simulated (the simulations included an additional random temperature error drawn from a distribution with mean zero and standard deviation

1 K) for the configurations shown in Table 3 are processed with an assumed cloud height and the results are binned according to the surface reflectance, the bias and standard error of the discrepancy between the recovered and the actual CO_2 column are as shown in the left-hand column of Figure 10. The rows refer to the cloud height used in the simulations, whereas the cloud was assumed to lie at 8.5 km in the inversion process. When the actual cloud is higher than the assumed cloud, the estimated Δu is biased low, and vice-versa. Generally, the standard deviation is highest for low reflectance, passes through a weak minimum near $r \approx 0.6$, and rises slightly for extremely bright surfaces. This behavior arises because glint is near the horizon, so the advantage of a brighter surface is outweighed by a longer atmospheric path and scattering closer to the forward lobe of the phase function.

[52] When the scattering level is estimated from O_2 data using parameterizations of the O_2–O_2 correlation stratified according to reflectance, as in equations (13) and (14), the estimation of CO_2 column u is more reliable, leading to the histograms in the right-hand column of Figure 10. The standard errors in Δu for cloud at all three levels generally are less than 0.5%, while the biases are small.

7. Conclusions

[53] Radiance measurements at two frequencies in the CO_2 absorption band at 1.61 μm in principle allow the CO_2 column to be estimated precisely in a clear atmosphere, but such is not the case in the presence of thin cloud and aerosol. Simulations based on a simple radiance model show that precision better than a few percent is unlikely, even when the optical thickness of cloud is as low as 0.02, because scattering by cirrus shortens the mean path lengths of photons reflected to space, and hence biases the estimate of the CO_2 column low. Simultaneous measurement of O_2 and CO_2 channels may provide a way to make the inversions more robust in the presence of modest amounts of cloud and aerosol. The O_2 channels allow the mean scattering level to be estimated, and the correlation between O_2 and CO_2 channels then allows the CO_2 column to be determined with precision approaching 0.5%. High spectral resolution is needed to avoid air glow in the 1.27 μm O_2 band.

[54] While these results are encouraging, issues canvassed only briefly in this paper that will need close investigation include the technical feasibility of high resolution spectroscopy, the effect of nonuniformity of the CO_2 volume mixing ratio, the accuracy of the spectroscopic data for CO_2 and O_2, and the variability of surface reflectance and scattering properties of cloud and aerosol between 1.27 μm and 1.61 μm. Mie calculations with ice spheres suggest that the latter is not a limiting factor, but calculations for more realistic ice clouds are required to confirm this result.

[55] **Acknowledgments.** The authors thank the anonymous reviewers for many constructive comments, including the suggestion that the analysis be based on the CO_2 line at 6205 cm^{-1} in order to avoid potential problems caused by solar lines near 6210 cm^{-1}.

References

Buchwitz, M., V. V. Rozanov, and J. P. Burrows, A near-infrared optimized DOAS method for the fast global retrieval of atmospheric CH_4, CO, CO_2, H_2O, and N_2O total column amounts from SCIAMACHY Envisat-1 nadir radiances, *J. Geophys. Res.*, *105*, 15,231–15,245, 2000.

Cox, C., and W. H. Munk, Statistics of the sea surface derived from Sun glitter, *J. Mar. Res.*, *13*, 198–227, 1954.

Edwards, D. P., GENLN2, a general line-by-line atmospheric transmittance and radiance model, *NCAR Tech. Note NCAR/TN-367 + STR*, Natl. Cent. for Atmos. Res., Boulder, Colo., 1992.

Engelen, R. J., A. S. Denning, K. R. Gurney, and G. L. Stephens, Global observations of the carbon budget, 1, Expected satellite capabilities for emission spectroscopy in the EOS and NPOESS eras, *J. Geophys. Res.*, *106*, 20,055–20,068, 2001.

Enting, I. G., C. M. Trudinger, and R. J. Francey, A synthesis inversion of the concentration and $\delta^{13}C$ of atmospheric CO_2, *Tellus, Ser. B*, *47*, 35–52, 1995.

Fu, Q., and Y. Takano, On the limitation of using asymmetry factor for radiative tranfer involving cirrus clouds, *Atmos. Res.*, *34*, 299–308, 1994.

Garrett, T. J., P. V. Hobbs, and H. Gerber, Shortwave, single-scattering properties of arctic ice clouds, Program in Atmos. and Oceanic Sci., Univ. of Colo., Boulder, 2000. (Available at http://paos.colorado.edu/curryja/wg5/specialpapers/Garrett/garrett_index.html).

Gerber, H., Y. Takano, T. J. Garrett, and P. V. Hobbs, Nephelometer measurements of the asymmetry parameter, volume extinction coefficient, and backscatter ratio in arctic clouds, *J. Atmos. Sci.*, *57*, 3021–3034, 2000.

Heidinger, A. K., and G. L. Stephens, Nadir sounding of clouds and aerosols in the O_2 A-band, *Atmos. Sci. Pap. 650*, Colorado State Univ., Fort Collins, Colo., 1998.

Henyey, L. G., and J. L. Greenstein, Diffuse radiation in the galaxy, *Astrophys. J.*, *93*, 70–83, 1941.

McClatchey, R. A., R. W. Fenn, J. E. A. Selby, F. E. Volz, and J. S. Garing, Optical properties of the atmosphere, 3rd ed., *Environ. Res. Pap. 411, AFCRL-72-0497*, Air Force Cambridge Res. Lab., Bedford, Mass., 1972.

Mischenko, M. I., and L. D. Travis, Light scattering by polydispersions of randomly oriented spheroids with sizes comparable to wavelengths of observation, *Appl. Opt.*, *33*, 7206–7225, 1994.

Noxon, J. F., A global study of the $O_2(^1\Delta_g)$ airglow: Day and twilight, *Planet. Space Sci.*, *10*, 545–557, 1982.

Rayner, P. J., and D. M. O'Brien, The utility of remotely sensed CO_2 concentration data in surface source inversions, *Geophys. Res. Lett.*, *28*, 175–178, 2001.

Rayner, P. J., I. G. Enting, R. J. Francey, and R. Langenfelds, Reconstructing the recent carbon cycle from atmospheric CO_2, $\delta^{13}C$ and O_2/N_2 observations, *Tellus, Ser. B*, *51*, 213–232, 1999.

Rodgers, C. D., *Inverse methods for atmospheric sounding, Atmospheric, Oceanic and Planetary Physics*, vol. 2, World Sci., River Edge, N. J., 2000.

Rothman, L. S., et al., The HITRAN molecular database edition of 1991 and 1992, *J. Quant. Spectrosc. Radiat. Transfer*, *48*, 469–507, 1992.

Smith, K. M., and D. A. Newnham, Near-infrared absorption cross sections and integrated absorption intensities of molecular oxygen (O_2, O_2–O_2, and O_2–N_2), *J. Geophys. Res.*, *105*, 7383–7396, 2000.

Takano, Y., and K.-N. Liou, Solar radiative transfer in cirrus clouds, part I, Single scattering and optical properties of hexagonal ice crystals, *J. Atmos. Sci.*, *46*, 3–19, 1989.

Tolton, B. T., and D. Plouffe, Sensitivity of radiometric measurements of the atmospheric CO_2 column from space, *Appl. Opt.*, *40*, 1305–1313, 2001.

Warren, S., Optical constants of ice from the ultraviolet to the microwave, *Appl. Opt.*, *23*, 1206–1225, 1984.

Wiscombe, W., Mie scattering code, NASA Goddard Space Flight Cent., Greenbelt, Md., 2000. (Available at ftp://climate.gsfc.nasa.gov/pub//wiscombe/Single_Scatt/Homogen_Sphere/Exact_Mie/MIEV0.f).

World Meteorological Organization (WMO), Final report, Exec. Council Panel of Experts on Satellites, Geneva, Switzerland, 1993. (Available at ftp://www.wmo.ch/Documents/www/sat/ecsatfrp.doc).

D. M. O'Brien and P. J. Rayner, CSIRO Atmospheric Research, Private Bag 1, Aspendale VIC 3195, Australia. (Denis.OBrien@dar.csiro.au)